Kim and Choi *EURASIP Journal on Wireless Communications and Networking* (2017) 2017:39
DOI 10.1186/s13638-017-0819-1

EURASIP Journal on Wireless Communications and Networking

RESEARCH Open Access

Iterative detection for frequency-asynchronous distributed Alamouti-coded (FADAC) OFDM

Bong-seok Kim[1] and Kwonhue Choi[2*]

Abstract

We propose a near intercarrier interference (ICI)-free and very low complexity iterative detector for frequency-asynchronous distributed Alamouti-coded (FADAC) orthogonal frequency division multiplexing (OFDM). In the previous cancelation schemes, the entire subcarrier signals from one transmit (TX) antenna are estimated and canceled in the received signal from the other TX antenna and vice versa. However, the reliability of the estimated symbols are revealed to significantly vary across the subcarriers and thus, the poorly estimated symbols lead to the incorrect cancelation. Motivated from this, we first propose a scheme which does not cancel the interfering subcarrier(s) at the half band edges which undergo very high interference in FADAC-OFDM. For further improvement, we propose a so-called selective scheme which instantly measures the reliability of the detected symbols at each iteration and then exclude the unreliable symbols in the estimated interference generation.
Moreover, the proposed scheme has a drastically reduced complexity by converting the cancelation process from the subcarrier domain to the time domain. In accordance with the analysis on the considered reliability measures, the numerical results show that the proposed scheme achieves the near ICI-free level only within three or four iterations for wide ranges of SNR, frequency offset, and delay spread.

Keywords: Iterative MIMO, Alamouti, ICI cancelation, OFDM, Distributed antennas, Frequency offset

1 Introduction

Recently, several studies on Alamouti-coded OFDM (orthogonal frequency division multiplexing) for cooperative systems have been reported. One of the main challenging issues in this area is to mitigate self-interference due to the carrier frequency offset (CFO) between the distributed transmit antennas [1–8]. Very recently in [4], the so-called FADAC-OFDM (frequency-asynchronous distributed Alamouti-coded OFDM) has been proposed and shown to outperform the other existing approaches in [3–5]. In contrast to the conventional distributed Alamouti-coded OFDM, FADAC-OFDM is free from ICI (intercarrier interference) terms from the near subcarriers due to its ICI self-cancelation property only by simple Alamouti-decoding process. Especially, [4] tried to exploit this ICI self-cancelation property even in the selective fading channel by dividing the entire subcarriers into multiple subblocks. However, in the severely frequency-selective fading channels, FADAC-OFDM gets worse due to non-negligible inter-block ICI terms.

Meanwhile, in [5–7], typical types of iterative ICI cancelation schemes for the conventional Alamouti-coded OFDM with the distributed antennas have been proposed. Since the conventional Alamouti-coded OFDM [9] has no ICI self-cancelation property for frequency and timing asynchronous distributed antennas, the accuracy of the initial detection is poor. Thus, a considerable number of iterations of cancelation has to be performed until the performance converges. Moreover, the converged performances are not so impressive. Although in [5] they derived the performance result close to no-CFO case, they assumed the perfect ICI cancelation which has not been justified. The schemes in [6, 7] rapidly break down as the CFO gets larger than 0.5. Moreover, they have high computation overheads because at each iteration, the required number of complex multiplications for the interference

*Correspondence: gonew@ynu.ac.kr
[2]Department of ICE in Yeungnam University, 280 Daehak-Ro, Gyeongsan, Gyeongbuk, 38541, Republic of Korea
Full list of author information is available at the end of the article

reconstruction is $4N^2$ where N denotes the total number of OFDM subcarriers.

Recently, in [10] and [14], the decision-directed iterative ICI cancelation schemes to distributed multiple input multiple output (MIMO) have been proposed. In [14], the authors considered spatial modulation MIMO as the application system model and they showed the performance results only for the small values of CFO. In [10], we, the authors of this paper, combined a typical decision-directed iterative ICI cancelation scheme to FADAC-OFDM. We achieved better performance compared with [5] even with low complexity due to better initial detection performance of FADAC-OFDM compared to the conventional Alamouti-coded OFDM. This scheme uses all the detected symbols in the interference reconstruction step without any consideration of reliability of detection symbols. However, even in FADAC-OFDM, some of the detection symbols may eventually have relatively high possibility of errors due to severe ICI terms such as inter-block ICI as mentioned before. It is shown that after the first iteration, the performance fairly improves, but from the second iteration, the performance is stuck in the same value. This is because the reconstructed interference term for cancelation is not updated anymore due to the erroneous portion of the constructed interference. Consequently, the performance gap between this scheme [10] and the case of no ICI is still considerable.

In order to solve drawbacks of the previous cancelation scheme [10], it is important to carefully decide whether or not to use each of the detected symbols in the interference reconstruction step at each iteration. In other words, we have to use or devise a certain measure to assess the reliability of the detected symbols at each iteration, based on which we have to exclude the unreliable symbols in the interference reconstruction.

To this end, we first propose a deterministic scheme where the fixed number of data symbols at the half band edges are not used in the interference reconstruction because they themselves undergo very high interference in FADAC-OFDM, and thus, they are less reliable. In order to further improve the cancelation performance, we propose a method which instantaneously measures the reliability of the soft detected symbols [12] at each iteration and then exclude the unreliable symbols in the estimated interference generation. We jointly employ two reliability check measures: (1) square error of the decision variable from the corresponding constellation point and (2) the detection consistency for two consecutive iterations.

Apart from the ICI cancelation performance itself, the computational complexity of the scheme should be feasible from the implementation viewpoint. In the proposed scheme, we employ a drastically low complexity structure which attains the complexity reduction in terms of polynomial order.

The remainder of this paper is structured as follows: First, we review FADAC-OFDM in Section 2. In Section 3, we first review our previous iterative cancelation scheme and its problem and then we propose two types of iterative cancelation schemes. In Section 4, we propose a complexity-reduced ICI cancelation structure. In Section 5, we provide the various performance results which support the improved ICI cancelation capability of the proposed schemes.

2 Review on FADAC-OFDM

In this paper, we are considering the iterative ICI cancelation schemes for FADAC-OFDM. In this section, we describe the motivation of FADAC-OFDM and give a self-contained review on the TX and receive (RX) structures of FADAC-OFDM. In addition, we revisit its residual ICI terms for the subsequent sections.

FADAC-OFDM has been proposed for FO-tolerant Alamouti-coded OFDM for frequency-asynchronous distributed antenna systems [4]. FADAC-OFDM employs a frequency reversal structure at the TX side. Then, FADAC-OFDM detects the symbols by performing simple linear combining after two separate DFT operations with local carriers synchronized to each TX antenna. By doing so, FADAC-OFDM cancels the major parts of intra-block ICI terms from neighboring subcarriers, and thus, FADAC-OFDM significantly improves the performance for the distributed antenna systems. However, despite the ICI self-cancelation property of FADAC-OFDM, two kinds of ICI terms, i.e., intra-block ICI and inter-block ICI, still remain non-negligible. This leads us to consider a further cancelation of the remaining ICI terms by using an iterative cancelation scheme which will be introduced in Section 3.

2.1 The system model and the OFDM symbol structure of FADAC-OFDM

In this section, we introduce the system model and the OFDM symbol structure of FADAC-OFDM. We consider the distributed antenna system that is composed of two TX antennas and one RX antenna. In each TX antenna, OFDM-modulated signals are transmitted with N total subcarriers, as in [1–6]. Let the variable $x_{b,l}$ denote the lth data symbol of the bth subblock and the variables $X_{b,k}^{(A)}$ and $X_{b,k}^{(B)}$ denote the Alamouti-coded symbols at the kth subcarrier of bth subblock of TX antennas A and B, respectively. Figures 1 and 2 show the OFDM symbol structures of the conventional distributed Alamouti-coded (CDAC) OFDM [5, 6] and FADAC-OFDM [4], respectively.

In CDAC-OFDM, Alamouti code pairs are mapped to the neighboring subcarriers just like the typical

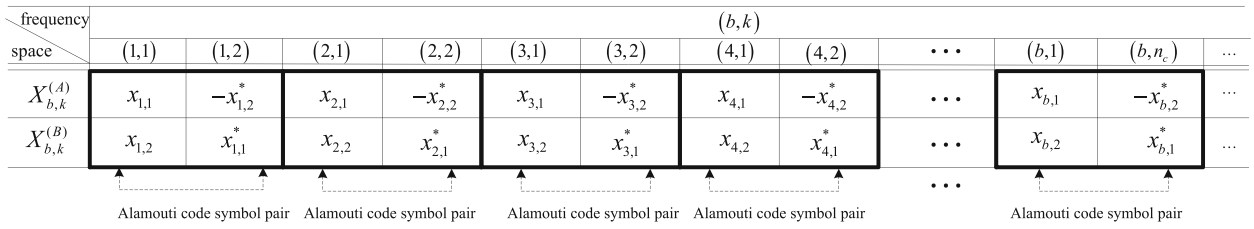

Fig. 1 OFDM symbol structure of CDAC-OFDM

space-frequency Alamouti code structure [15], i.e., $X_{b,k}^{(A)}$ and $X_{b,k}^{(B)}$ are set to

$$X_{b,k}^{(A)} = \begin{cases} x_{b,1} & \text{if } k = 1, \\ -x_{b,2}^{*} & \text{if } k = 2, \end{cases} \tag{1}$$

$$X_{b,k}^{(B)} = \begin{cases} x_{b,2} & \text{if } k = 1, \\ x_{b,1}^{*} & \text{if } k = 2, \end{cases} \tag{2}$$

where $x_{b,1}$ and $x_{b,2}$ denote the two data symbols for the bth subblock.

Meanwhile, in FADAC-OFDM, the subblock size (the number of subcarriers per subblock) is larger than 2, and then, Alamouti-coded symbol pairs are packed into the mirror images in each subblock as shown in Fig. 2. Specifically, N-total subcarriers are partitioned into N_b subblocks, and thus, the block size n_c is equal to N/N_b. Thus, in FADAC-OFDM, $X_{b,k}^{(A)}$ and $X_{b,k}^{(B)}$ for $1 \le b \le N_b$ are set as follows:

$$X_{b,k}^{(A)} = \begin{cases} x_{b,2k-1} & \text{for } 1 \le k \le n_c/2, \\ -x_{b,2(n_c-k+1)}^{*} & \text{for } n_c/2+1 \le k \le n_c, \end{cases} \tag{3}$$

$$X_{b,k}^{(B)} = \begin{cases} x_{b,2k} & \text{for } 1 \le k \le n_c/2, \\ x_{b,2(n_c-k)+1}^{*} & \text{for } n_c/2+1 \le k \le n_c. \end{cases} \tag{4}$$

We assume that the fading is locally flat over the Alamouti-coded block. To justify this assumption, the block size n_c is set smaller than the coherent bandwidth. From Figs. 1 and 2, it is straightforward that as an extreme case, the FADAC-OFDM with $n_c = 2$ is equivalent to CDAC-OFDM.

2.2 RX structure of FADAC-OFDM

Figure 3 shows the overall structures for the previous and the proposed ICI cancelation schemes, which will be explained later. The parts inside the bold boxes which are common to both structures correspond to the RX structure of FADAC-OFDM. We assume that there exists an inevitable carrier frequency offset (CFO) between $f_c^{(A)}$ and $f_c^{(B)}$ which denote the received carrier frequencies from distributed TX antennas A and B, respectively. Two FFTs (fast Fourier transforms) are performed on the RX signal by separately synchronizing to two asynchronous TX antennas' carrier frequencies and arrival timings.

Let the variables $\mathbf{r}^{(A)}$ and $\mathbf{r}^{(B)}$ denote two FFT input vectors synchronized to TX antennas A and B, respectively, as shown in Fig. 3, then the FFT outputs corresponding to the kth elements of the bth subblock of two TX antennas are expressed as [10]

$$R_{b,k}^{(A)} = H_{b,k}^{(A)} X_{b,k}^{(A)} + I_{b,k}^{(A)} + w_{b,k}^{(A)} \tag{5}$$

$$R_{b,k}^{(B)} = H_{b,k}^{(B)} X_{b,k}^{(B)} + I_{b,k}^{(B)} + w_{b,k}^{(B)} \tag{6}$$

where $w_{b,k}^{(A)}$ and $w_{b,k}^{(B)}$ are AWGN terms and $H_{b,k}^{(A)}$ and $H_{b,k}^{(B)}$ are channel fading coefficients at the kth subcarrier of the bth subblock from TX antennas A and B, respectively, and they are each independent and follow zero mean, unit variance complex Gaussian distribution.

The variables $I_{b,k}^{(A)}$ and $I_{b,k}^{(B)}$ denote ICI terms due to CFO and they are expressed as follows:

$$I_{b,k}^{(A)} = \sum_{\beta=1}^{N_b} \sum_{m=1}^{n_c} Q\left(\left(\beta - b\right) n_c + m - \varepsilon - k\right) H_{\beta,m}^{(B)} X_{\beta,m}^{(B)}, \tag{7}$$

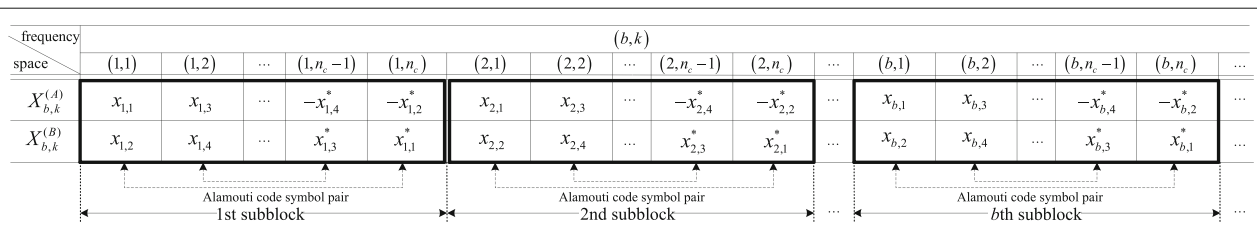

Fig. 2 OFDM symbol structure of FADAC-OFDM

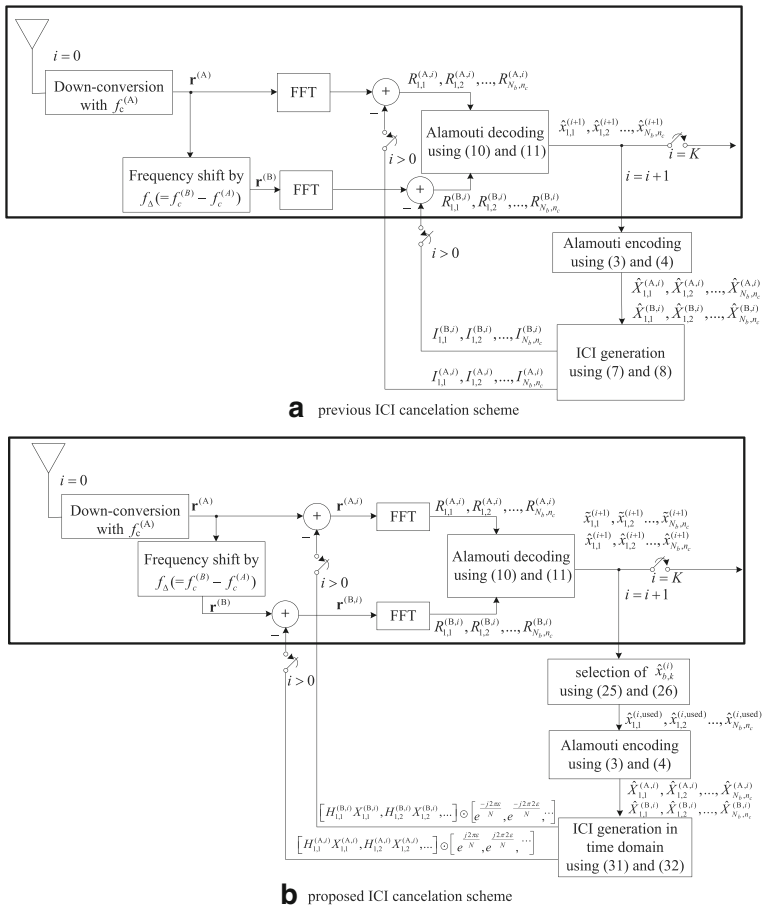

Fig. 3 Receiver structures for the previous scheme in [10] (**a**) and the proposed scheme (**b**)

$$I_{b,k}^{(B)} = \sum_{\beta=1}^{N_b} \sum_{m=1}^{n_c} Q\left(\left(\beta - b\right) n_c + m + \varepsilon - k\right) H_{\beta,m}^{(A)} X_{\beta,m}^{(A)} \tag{8}$$

where ε is the normalized CFO between two transmit antennas, i.e., $\varepsilon = (f_c^{(B)} - f_c^{(A)})/f_\Delta$ where f_Δ is the subcarrier spacing and $Q(x)$ is the ICI coefficient given as [16]

$$Q(x) = \frac{\sin(\pi x)}{N \sin((\pi/N)x)} \exp\left[j\pi(1 - 1/N)x\right]. \tag{9}$$

With a typical Alamouti decoding, the normalized decision variables (DVs) $\tilde{x}_{b,2k-1}$ and $\tilde{x}_{b,2k}$ corresponding to $x_{b,2k-1}$ and $x_{b,2k}$, respectively, are obtained as follows:

$$\tilde{x}_{b,2k-1} = \frac{H_{b,k}^{*(A)} R_{b,k}^{(A)} + H_{b,n_c-k+1}^{(B)} R_{b,n_c-k+1}^{*(B)}}{\left|H_{b,k}^{(A)}\right|^2 + \left|H_{b,n_c-k+1}^{(B)}\right|^2}, \tag{10}$$

$$\tilde{x}_{b,2k} = \frac{H_{b,k}^{*(B)} R_{b,k}^{(B)} - H_{b,n_c-k+1}^{(A)} R_{b,n_c-k+1}^{*(A)}}{\left|H_{b,k}^{(B)}\right|^2 + \left|H_{b,n_c-k+1}^{(A)}\right|^2}. \tag{11}$$

Substituting (5) and (6) into (10), with $X_{b,k}^{(A)}$ and $X_{b,k}^{(B)}$ replaced by (3) and (4), results in $\tilde{x}_{b,2k-1}$ as the summation of the data symbol $x_{b,2k-1}$ and degrading effect terms, i.e., interference term $i_{b,2k-1}$ and noise term $w_{b,2k-1}$, respectively, as follows [4]:

$$\begin{aligned}\tilde{x}_{b,2k-1} = x_{b,2k-1} &+ \underbrace{\frac{H_{b,k}^{*(A)} I_{b,k}^{(A)} + H_{b,n_c-k+1}^{(B)} I_{b,n_c-k+1}^{*(B)}}{\left|H_{b,k}^{(A)}\right|^2 + \left|H_{b,n_c-k+1}^{(B)}\right|^2}}_{\text{interference term}, \triangleq i_{b,2k-1}} \\ &+ \underbrace{\frac{H_{b,k}^{*(A)} w_{b,k}^{(A)} + H_{b,n_c-k+1}^{(B)} w_{b,n_c-k+1}^{*(B)}}{\left|H_{b,k}^{(A)}\right|^2 + \left|H_{b,n_c-k+1}^{(B)}\right|^2}}_{\text{noise term}, \triangleq w_{b,2k-1}}.\end{aligned} \tag{12}$$

In (12), $w_{b,2k-1}$ still follows Gaussian distribution because $w_{b,2k-1}$ is the linear combination of two i.i.d noise samples with the same weighting factors. Therefore, $w_{b,2k-1}$ has the identical static to that of $w_{b,k}^{(A)}$ and

$w^{*(B)}_{b,n_c-k+1}$. Meanwhile, substituting (7) and (8) into $i_{b,2k-1}$ in (12), $i_{b,2k-1}$ is expressed as the summation of the intra-block ICI and inter-block ICI terms, as follows:

$$i_{b,2k-1} = \underbrace{\left(\begin{array}{l} H^{*(A)}_{b,k} \sum_{m=1}^{n_c} Q(m+\varepsilon-k) H^{(B)}_{b,m} X^{(B)}_{b,m} \\ +H^{(B)}_{b,n_c-k+1} \sum_{m=1}^{n_c} Q(m-\varepsilon-(n_c-k+1)) H^{*(A)}_{b,m} X^{*(A)}_{b,m} \end{array} \right)}_{\triangleq i^{\text{intra}}_{b,2k-1},\ \text{intra - block ICI}}$$
$$+ \underbrace{\left(\begin{array}{l} H^{*(A)}_{b,k} \sum_{\beta\neq b}^{N_b} \sum_{m=1}^{n_c} Q((\beta-b)n_c+m+\varepsilon-k) H^{(B)}_{\beta,m} X^{(B)}_{\beta,m} \\ +H^{(B)}_{b,n_c-k+1} \times \\ \sum_{\beta\neq b}^{N_b} \sum_{m=1}^{n_c} Q((\beta-b)n_c+m-\varepsilon-(n_c-k+1)) H^{*(A)}_{\beta,m} X^{*(A)}_{\beta,m} \end{array} \right)}_{\triangleq i^{\text{inter}}_{b,2k-1},\text{inter-block ICI}}. \quad (13)$$

We assume that the block size n_c is set smaller than coherent bandwidth, that is, the fading is locally flat over the Alamouti-coded block. By our assumption, $H^{(A)}_{b,k}$ and $H^{(B)}_{b,k}$ are replaced by $H^{(A)}_b$ and $H^{(B)}_b$, respectively. Therefore, $i^{\text{intra}}_{b,2k-1}$ is expressed as the summation of the four interference terms $i^{\text{intra},(1)}_{b,2k-1}$, $i^{\text{intra},(2)}_{b,2k-1}$, $i^{\text{intra},(3)}_{b,2k-1}$, and $i^{\text{intra},(4)}_{b,2k-1}$, as follows [4]:

$$\begin{aligned} i^{\text{intra}}_{b,2k-1} &= \underbrace{H^{*(A)}_b H^{(B)}_b \sum_{m=1}^{n_c/2} Q(m+\varepsilon-k) X^{(B)}_{b,m}}_{\triangleq i^{\text{intra},(1)}_{b,2k-1}} \\ &+ \underbrace{H^{*(A)}_b H^{(B)}_b \sum_{m=n_c/2+1}^{n_c} Q(m+\varepsilon-k) X^{(B)}_{b,m}}_{\triangleq i^{\text{intra},(2)}_{b,2k-1}} \\ &+ \underbrace{H^{*(A)}_b H^{(B)}_b \sum_{m=1}^{n_c/2} Q(m-\varepsilon-(n_c-k+1)) X^{*(A)}_{b,m}}_{\triangleq i^{\text{intra},(3)}_{b,2k-1}} \\ &+ \underbrace{H^{*(A)}_b H^{(B)}_b \sum_{m=n_c/2+1}^{n_c} Q(m-\varepsilon-(n_c-k+1)) X^{*(A)}_{b,m}}_{\triangleq i^{\text{intra},(4)}_{b,2k-1}}. \end{aligned} \quad (14)$$

Figure 4 shows the variances of the four interference terms mentioned above for $\varepsilon = 0.2$ and $\varepsilon = 0.5$. Intuitively, the variances of $i^{\text{intra},(1)}_{b,2k-1}$ and $i^{\text{intra},(4)}_{b,2k-1}$ are identical and the variances of $i^{\text{intra},(2)}_{b,2k-1}$ and $i^{\text{intra},(3)}_{b,2k-1}$ are identical. Note that the variances of $i^{\text{intra},(1)}_{b,2k-1}$ and $i^{\text{intra},(4)}_{b,2k-1}$ are significantly dominant over those of $i^{\text{intra},(2)}_{b,2k-1}$ and $i^{\text{intra},(3)}_{b,2k-1}$. This is because $i^{\text{intra},(1)}_{b,2k-1}$ and $i^{\text{intra},(4)}_{b,2k-1}$ are the ICI from the subcarriers of the half subblock where the desired subcarrier

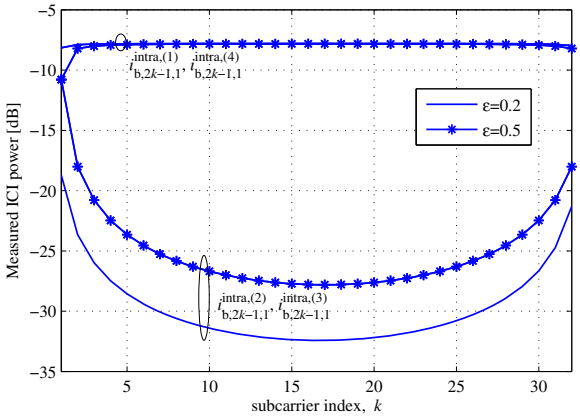

Fig. 4 The variances of the four terms in intra-block ICI with $n_c = 32$ for $\varepsilon = 0.2$ and $\varepsilon = 0.5$

belongs to, whereas $i^{\text{intra},(2)}_{b,2k-1}$ and $i^{\text{intra},(3)}_{b,2k-1}$ are the ICI from the other half subblock [4].

Let us focus on one of the dominant intra-block ICI terms $i^{\text{intra},(4)}_{b,2k-1}$. From (9), $Q(x) = Q^*(-x)$, and thus, $Q^*(-(m-\varepsilon-k)) = Q(m+\varepsilon-k)$, and from (3) and (4), $X^{(A)}_{b,n_c-m+1} = -X^{*(B)}_{b,m}$. Using these properties and introducing a new indexing variable, i.e., $m' = n_c - m + 1$ to rearrange $n_c/2 + 1 \le m \le n_c$ in reverse order, $i^{\text{intra},(4)}_{b,2k-1}$ in (14) can be rewritten as

$$\begin{aligned} i^{\text{intra},(4)}_{b,2k-1} &= H^{*(A)}_b H^{(B)}_b \sum_{m'=1}^{n_c/2} Q^*(n_c-m'+1-\varepsilon \\ &\quad -(n_c-k+1)) X^{*(A)}_{b,n_c-m'+1} \\ &= H^{*(A)}_b H^{(B)}_b \sum_{m=1}^{N/2} Q^*(-m-\varepsilon+k) \left(-X^{*(B)}_{b,m}\right)^* \\ &= -H^{*(A)}_b H^{(B)}_b \sum_{m=1}^{N/2} Q(m+\varepsilon-k) X^{(B)}_{b,m} \\ &= -i^{\text{intra},(1)}_{2k-1} \end{aligned} \quad (15)$$

which concludes that $i^{\text{intra},(1)}_{b,2k-1}$ and $i^{\text{intra},(4)}_{b,2k-1}$ in (14) cancel each other. By canceling $i^{\text{intra},(1)}_{b,2k-1}$ and $i^{\text{intra},(4)}_{b,2k-1}$ which are dominant terms in intra-block ICI, the performance degradation due to ICI can be substantially ameliorated. On the other hand, we can show that $i^{\text{intra},(2)}_{2k-1} = i^{\text{intra},(3)}_{2k-1}$ without difficulty, and thus, the overall intra-block ICI term $i^{\text{intra}}_{b,2k-1}$ can be expressed as the relatively weak ICI term $i^{\text{intra},(2)}_{b,2k-1}$ as follows:

$$\begin{aligned} i^{\text{intra}}_{b,2k-1} &= 2H^{*(A)}_b H^{(B)}_b \sum_{m=n_c/2+1}^{n_c} Q(m-\varepsilon-k) X^{(B)}_{b,m} \\ &= 2i^{\text{intra},(2)}_{b,2k-1}. \end{aligned} \quad (16)$$

Therefore, (12) is rewritten as the summation of the data symbol, the minor part of the intra-block ICI term, inter-block ICI term, and additive noise term, as follows:

$$\tilde{x}_{b,2k-1} = x_{b,2k-1} + 2i_{b,2k-1}^{\text{intra},(2)} + i_{b,2k-1}^{\text{inter}} + w_{b,2k-1} \quad (17)$$

Using a similar calculation and notation, $x_{b,2k}$ is represented without difficulty and loss of generality as

$$\tilde{x}_{b,2k} = x_{b,2k} + 2i_{b,2k}^{\text{intra},(2)} + i_{b,2k}^{\text{inter}} + w_{b,2k}. \quad (18)$$

Figure 5a shows the normalized average ICI powers in the decision variables according to the pair of subblock number and subcarrier index, i.e., (b,k) with $N = 256$ and $n_c = 32$. The term i in the legend denotes the number of the iterative cancelations whose detailed algorithm will be proposed in the subsequent subsection. In Fig. 5a, it is shown that even without the iterative cancelation ($i = 0$), the ICI power of FADAC-OFDM is maintained lower than -15 dB in the middle of half subblocks even for a large ε, i.e., 0.5. This is due to the intrinsic property of FADAC-OFDM, i.e., the major ICI terms from the neighboring subcarriers in the considered subblock are completely self-canceled. Meanwhile, despite intra-block ICI self-cancelation, the ICI power sharply increases at the half band edges ($k = n_c/2$ or $k = n_c$). This is because in the vicinity of the half subblock edges, the frequency distances between the considered subcarrier and the subcarriers belonging to the counterpart (the other side) half subblock or the consecutive subblocks decrease and the interferences from these subcarriers are not canceled by FADAC-OFDM as shown in (17) and (18).

Motivated from this, by using an iterative cancelation step which will be introduced in the next section, we try to cancel further the remaining ICI terms. In Fig. 5a, by employing iterative cancelation, it is shown that ICI powers at half band edge and band edge significantly decrease compared to the case before iterative cancelation. However, the ICI powers at half subblock edges are still relatively large compared to the middle band. This is because the iterative ICI cancelation is not perfect, and thus, the reason for high interferences at the half subblock edges mentioned above still holds.

For a reference, Fig. 5b shows the normalized ICI power of FADAC-OFDM with $n_c = 2$ which is equivalent to CDAC-OFDM. With $n_c = 2$, the feature of FADAC-OFDM, i.e., self-cancelation of the intra-block ICI term, is meaningless because there exists only one subcarrier in each half subblock. Thus, the ICI powers over all subcarriers are very high as shown in Fig. 5b, and the iterative cancelation is not so effective either. This implies that CDAC-OFDM is not suitable for the frequency-asynchronous distributed antenna systems.

Figure 6 shows the bit error rate (BER) results of FADAC-OFDM according to the subblock size n_c with $\varepsilon = 0.5$ for the several cases of $T_{\max}$ which denotes the maximum delay spread of multi-path, and T denotes the OFDM symbol duration. It is shown that the optimal n_c is larger than 2 and is getting larger as the delay spread decreases, which accords with our expectation. In addition, as the delay spread decreases, the suboptimal zone where the performance is rather insensitive to n_c is getting wider. However, if n_c is set excessively large, the performance is getting worse.

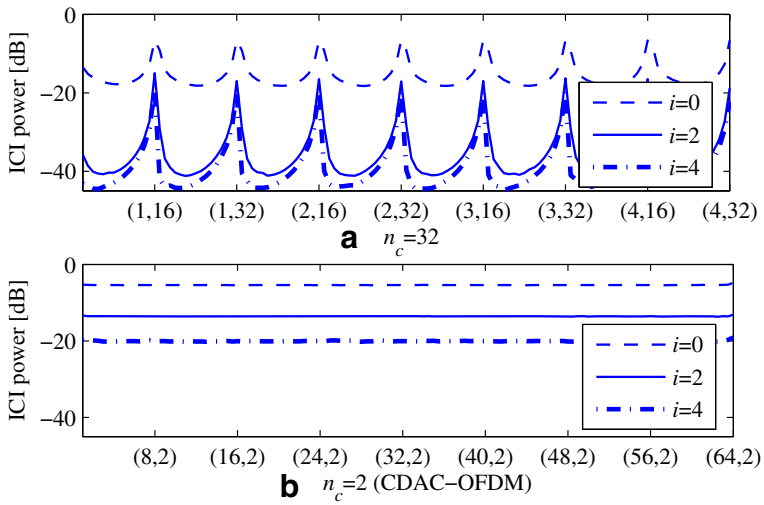

Fig. 5 Normalized average ICI power in decision variables of FADAC-OFDM with $n_c = 32$ (**a**) and $nc = 2$ (CDAC-OFDM) (**b**), according to the pair of subblock number and subcarrier index and the number of iterations for cancelation i, $\varepsilon = 0.5$ and $N = 256$

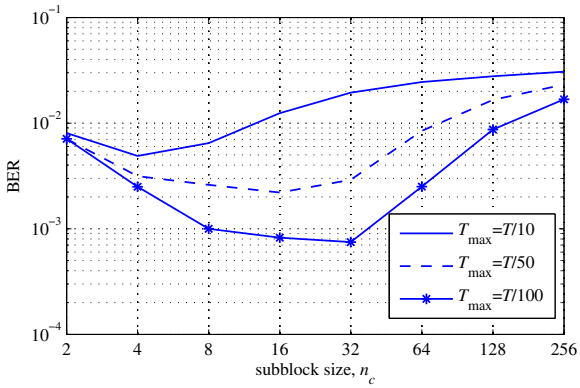

Fig. 6 The BER results according to n_c for the several T_{max}s, $\varepsilon = 0.5$ for BPSK with $E_b/N_0 = 20$ dB

3 Combining iterative ICI cancelation schemes to FADAC-OFDM

3.1 The previous iterative ICI cancelation scheme for FADAC-OFDM

The procedure of the previous iterative ICI cancelation scheme to FADAC-OFDM in [10] is shown in Fig. 3a. First, FADAC-OFDM is performed for initial detection. Then, the estimated ICI terms are generated by using initial detection symbols and channel information to subtract ICI terms from RX signal. This is iteratively performed by updating the detection symbols at each iteration. Denote $\hat{x}_{b,2k-1}^{(i)}$ and $\hat{x}_{b,2k}^{(i)}$ as the detection symbols obtained by slicing $\tilde{x}_{b,2k-1}$ and $\tilde{x}_{b,2k}$ in (17) and (18), respectively, at the ith iteration. By substituting $\hat{x}_{b,2k-1}^{(i)}$ and $\hat{x}_{b,2k}^{(i)}$ into (3) and (4) and then into (7) and (8), we reconstruct the estimated versions of $I_{b,k}^{(A)}$ and $I_{b,k}^{(B)}$, respectively, at the ith iteration. Denote $\hat{I}_{b,k}^{(A)}(i)$ and $\hat{I}_{b,k}^{(B)}(i)$ as the estimated versions of $I_{b,k}^{(A)}$ and $I_{b,k}^{(B)}$ at the ith iteration, respectively. We update the FFT outputs $R_{b,k}^{(A)}$ and $R_{b,k}^{(B)}$ at the ith iteration as follows:

$$R_{b,k}^{(A,i)} \leftarrow R_{b,k}^{(A)} - \hat{I}_{b,k}^{(A,i)}, \tag{19}$$

$$R_{b,k}^{(B,i)} \leftarrow R_{b,k}^{(B)} - \hat{I}_{b,k}^{(B,i)}, \tag{20}$$

where $R_{b,k}^{(A,i)}$ and $R_{b,k}^{(B,i)}$ denote the updated versions of $R_{b,k}^{(A)}$ and $R_{b,k}^{(B)}$, respectively, at the ith iteration. Finally, at each iteration, we perform the Alamouti combining in (10) and (11) using $R_{b,k}^{(A,i)}$ and $R_{b,k}^{(B,i)}$ to obtain the updated detection symbols $\hat{x}_{b,2k-1}^{(i+1)}$ and $\hat{x}_{b,2k}^{(i+1)}$, respectively, for the next $((i+1)$th) iteration.

In [10], it is shown that due to the good performance of FADAC-OFDM by intra-subblock ICI self-cancelation, this basic iterative scheme for FADAC-OFDM achieves better performance with lower complexity compared with [5]. However, this scheme still has room to be improved. Due to high ICI power at the subband edges shown in Fig.5, the detection symbols at those edges are more likely to be erroneously detected compared to the other detection symbols. The incorrect detection symbols result in the incorrect ICI term reconstruction and thus the incorrect ICI cancelation. As a result, even with increasing iterations, the improvement of performance is limited and the error probability is stuck in a certain point where the non-negligible incorrect contribution to the reconstructed ICI term is not self-corrected by the iterations any more. This will be checked out again in the simulation results.

3.2 The proposed iterative ICI cancelation schemes

In the previous section, we addressed the issue of the previous iterative ICI cancelation in [10], i.e., the drawback of using the entire detection symbols for ICI reconstruction and cancelation. To tackle this issue, we propose two types of selective ICI cancelation schemes.

3.2.1 Scheme I. DS scheme

As the first scheme to avoid the problem of using the unreliable symbol detection at the subband edges, we simply do not use the fixed number of symbols at the subband edges for ICI term reconstruction. In other words, if we denote $\hat{x}_{b,2k-1}^{(i,\text{used})}$ and $\hat{x}_{b,2k}^{(i,\text{used})}$ as the symbol estimates which will be finally used to reconstruct the ICI terms for cancelation at the ith iteration, they are set as follows:

$$\hat{x}_{b,2k-1}^{(i,\text{used})} = \begin{cases} 0 & \text{if } k \in E \\ \hat{x}_{b,2k-1}^{(i)}, & \text{elsewhere} \end{cases}, \tag{21}$$

$$\hat{x}_{b,2k}^{(i,\text{used})} = \begin{cases} 0 & \text{if } k \in E \\ \hat{x}_{b,2k}^{(i)}, & \text{elsewhere} \end{cases}, \tag{22}$$

where E is a set of indices of edge subcarriers, i.e., $E = \{1, 2, \ldots, M, \frac{n_c}{2} - M + 1, \frac{n_c}{2} - M + 2, \ldots, \frac{n_c}{2}\}$, and M is the number of data symbols (subcarriers) at each edge to be excluded in the ICI term reconstruction. For example, if M is set to 2 with $n_c = 16$, then set E is equal to $\{1, 2, 7, 8\}$. Consequently, $2M(=M$ pairs of Alamouti code) data symbols are not used, and they are replaced by null data symbols in the ICI term reconstruction. Simply by excluding $2M$ detection symbols at the edge in each subblock which are severely interfered by inter-block ICIs, we can avoid the performance degradation due to wrong ICI term cancelation. Another merit of this scheme is that it does not need any additional hardware or computations compared to [10].

This scheme excludes the data symbols in the deterministic carrier positions, i.e., predetermined positions based on the average ICI power distribution across the subcarriers as shown in Fig. 5. However, we know from (7) and (8) that the ICI term at each subcarrier contains lots of random variables such as the data symbols in the other subcarriers and their fading coefficients and thus the

ICI power at each subcarrier instantaneously varies. This implies that some of the edge subcarriers can eventually undergo rather small instantaneous ICI despite the high average ICI power. As we need the instantaneous reliability of the detection symbols to decide whether or not to use each detection symbol, the proposed DS (deterministically selective) scheme which simply excludes the fixed number of band edge subcarriers still has room to be improved if we can accommodate the instantaneous reliability of the detection symbols.

3.2.2 Scheme II. AS scheme

To alleviate the problem of the proposed DS scheme mentioned in the previous paragraph, we propose another so-called adaptively selective (AS) scheme. In the proposed AS scheme, we use two measures for the instantaneous reliability of the detection symbols. As one of the reliability measures, we use the square error between the soft decision variable $\tilde{x}$ and its nearest constellation point $\hat{x}$ as the tentative decision value [11]. Let us denote this reliability measure for a certain detection symbol $\hat{x}$ by γ, then it is calculated as

$$\gamma = |\tilde{x} - \hat{x}|^2. \tag{23}$$

In order to check whether or not this measure well reflects the reliability of the detection symbol, we simulated the cumulative distribution function (CDF) of γ for the correct detection case and the incorrect detection case. Figure 7 shows CDFs of γ for two (correct and incorrect) cases when $N = 256$ and $n_c = 16$. It is clear in Fig. 7 that γ for the correct case is distributed in the quite low range whereas γ for the incorrect case is distributed in the quite high range. For example, in the initial ($i = 0$) detection, for the correct detection case, 96% of γs is smaller than 0.5 whereas for the incorrect detection case, 95% of γs is larger than 0.5. This feature becomes even more remarkable as the iteration goes on. This implies that by simply comparing γ with a threshold, we can properly measure the reliability of the corresponding detection symbol. We use the following criterion to decide whether or not to use the detection symbol in the ICI reconstruction.

$$\hat{x}^{(\text{used})} = \begin{cases} \hat{x}, & \text{if } \gamma \le \rho \\ 0, & \text{else} \end{cases} \tag{24}$$

where $\hat{x}^{(\text{used})}$ denotes the actual value which will be used in the ICI reconstruction and ρ is a threshold value which determines whether or not the detection is sufficiently reliable or not.

Note in Fig. 7 that this criterion possibly misses the correct symbols or possibly uses the incorrect symbols in the ICI reconstruction step. The threshold ρ should be set by considering both of these two possibilities. The optimum value will vary according to the channel parameters, the system parameters, or even the iteration layer. However, in the practical system, it is likely to use, rather, a constant threshold, i.e., global suboptimal setting, and thus, we cannot avoid the performance loss compared to the optimized case.

To complement this, we use another measure to assess the reliability of the detection symbols, i.e., detection consistency between two consecutive iterations. If a certain detection symbol is sufficiently reliable at the ith iteration, the detection result would not change in the $(i+1)$th iteration. Hence, we treat a detection symbol as the reliable one if its detection result is maintained between two consecutive iterations. This measure well compromises the probability that the first criterion in (24) uses the incorrect symbol(s) in the ICI reconstruction step. For example, when a certain incorrect detection symbol has a small γ,

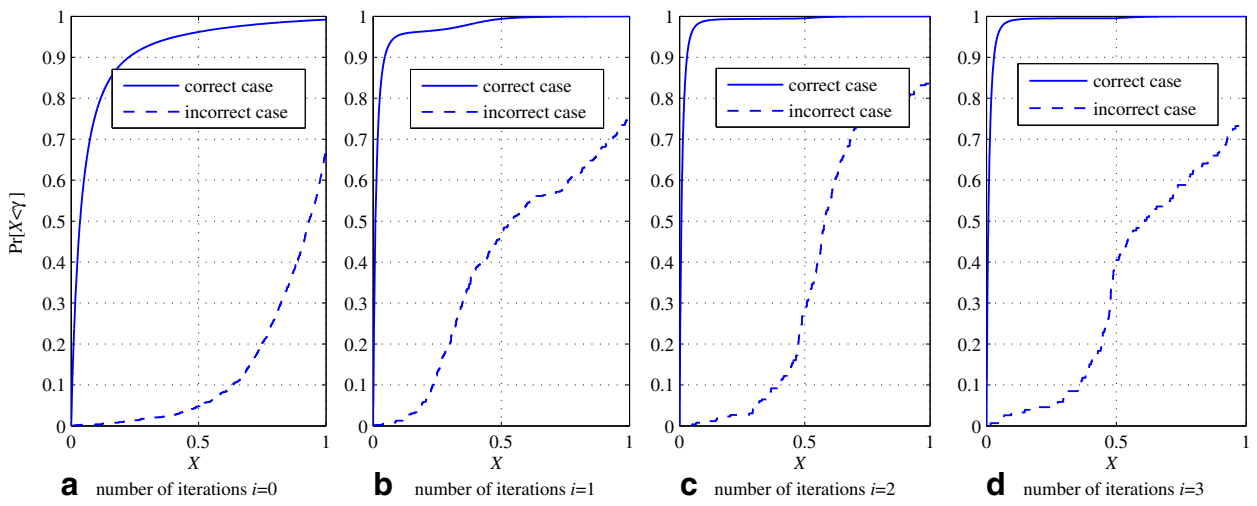

Fig. 7 a–d CDF of γ at each iteration

we conclude that it eventually has the small γ and it is unreliable if the detection result in the previous iteration is not equal to the detection result in the current iteration.

Summing up, the proposed AS scheme uses the following criterion for selecting the detection symbols in the ICI reconstruction step.

$$\hat{x}_{b,2k-1}^{(i,\text{used})} = \begin{cases} \hat{x}_{b,2k-1}^{(i)}, & \text{if } \gamma_{b,2k-1}^{(i)} \le \rho, \\ 0, & \text{else} \end{cases} \quad \text{for } i < 2$$
$$\begin{cases} \hat{x}_{b,2k-1}^{(i)}, & \text{if } \hat{x}_{b,2k-1}^{(i)} = \hat{x}_{b,2k-1}^{(i-1)} \text{and } \gamma_{b,2k-1}^{(i)} \le \rho, \\ 0, & \text{else} \end{cases} \quad \text{for } i \ge 2, \tag{25}$$

$$\hat{x}_{b,2k}^{(i,\text{used})} = \begin{cases} \hat{x}_{b,2k}^{(i)}, & \text{if } \gamma_{b,2k}^{(i)} \le \rho, \\ 0, & \text{else} \end{cases} \quad \text{for } i < 2$$
$$\begin{cases} \hat{x}_{b,2k}^{(i)}, & \text{if } \hat{x}_{b,2k}^{(i)} = \hat{x}_{b,2k}^{(i-1)} \text{and } \gamma_{b,2k}^{(i)} \le \rho, \\ 0, & \text{else} \end{cases} \quad \text{for } i \ge 2. \tag{26}$$

In order to check whether or not the two conditions in (25) and (26) well discriminate the correct or incorrect detections, we have to see the two kinds of conditional probabilities: (1) $p_{\text{false}}^{\text{condition}}$ denoting the probability of incorrect symbol detection despite the condition being satisfied ("false rate" in short) and (2) $p_{\text{miss}}^{\text{condition}}$ denoting the probability of correct symbol detection despite the condition being unsatisfied ("miss rate" in short). First, $p_{\text{false}}^{\text{condition}}$ for two conditions are written as follows:

$$p_{\text{false}}^{\text{C1}} = \Pr\left[\hat{x}_{b,2k-1}^{(i)} \ne x_{b,2k-1} | \gamma_{b,2k-1}^{(i)} \le \rho\right] \tag{27}$$
$$p_{\text{false}}^{\text{C2}} = \Pr\left[\hat{x}_{b,2k-1}^{(i)} \ne x_{b,2k-1} | \hat{x}_{b,2k-1}^{(i)} = \hat{x}_{b,2k-1}^{(i-1)}\right] \tag{28}$$

and $p_{\text{miss}}^{\text{condition}}$ for two conditions are written as follows:

$$p_{\text{miss}}^{\text{C1}} = \Pr\left[\hat{x}_{b,2k-1}^{(i)} = x_{b,2k-1} | \gamma_{b,2k-1}^{(i)} > \rho\right] \tag{29}$$
$$p_{\text{miss}}^{\text{C2}} = \Pr\left[\hat{x}_{b,2k-1}^{(i)} = x_{b,2k-1} | \hat{x}_{b,2k-1}^{(i)} \ne \hat{x}_{b,2k-1}^{(i-1)}\right] \tag{30}$$

where C1 denotes the condition $\gamma_{b,2k-1}^{(i)} \le \rho$ and C2 denotes the condition $\hat{x}_{b,2k-1}^{(i)} = \hat{x}_{b,2k-1}^{(i-1)}$. As the similar expressions hold for $x_{b,2k}$, we exclude the expressions for $x_{b,2k-1}$ without loss of generality. To avoid the wrong cancelation, we have to lower $p_{\text{false}}^{\text{condition}}$, and to avoid missing the correct detection symbols, we have to lower $p_{\text{miss}}^{\text{condition}}$.

Figure 8 shows the four conditional probabilities in (27)–(30) with $\rho = 0.4$ and $\varepsilon = 0.5$. Due to symmetry, $x_{b,2k}$ should have the same results. The condition C1 has smaller false rate but much larger miss rate compared to the condition C2. We can expect the performance improvement by jointly using the two conditions. To confirm this, the results for the joint condition $\{C1 \bigcap C2\}$ which is adopted in the proposed AS scheme are also plotted in Fig. 8. Note that this joint condition achieves much lower miss rate than that of using the condition C1 alone while achieving the false rate as low as that of using the condition C1 alone. Compared to the condition C2, the joint condition has the similar level of miss rate in the practically high (signal-to-noise ratio) SNR region while achieving quite smaller false rate.

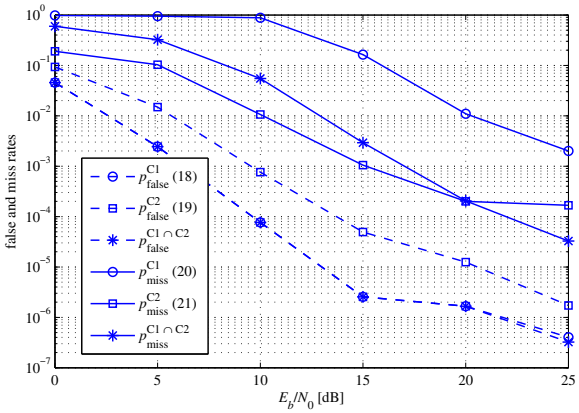

Fig. 8 False and miss rates, $\rho = 0.4, \varepsilon = 0.5$

4 Complexity reduction

The hardware structures of the iterative cancelations in [5–7, 10] are basically the same. They all include the calculations for reconstructing the interference term at each FFT outputs expressed in (7) and (8) at each iteration. The interference term in (7) and (8) have $2N$ complex multiplications. As there are two FFTs with N outputs, the overall required number of complex calculations for interference term reconstruction per iteration is equal to $4N^2$.

Meanwhile in the proposed scheme, we modify this complexity-expensive structure into a mathematically equivalent but low complexity structure. Figure 3 shows the receiver structures for the previous iterative cancelation scheme in [10] and the proposed scheme. Instead of performing cancelation at the FFT output stage (subcarrier domain), we can equivalently cancel the interference at the FFT input stage (time domain). Hence, the reconstructed interference corresponds to the time domain version. The reduced computation is intuitive due to the fact that the time domain interference takes the form of just a single sampled vector but it contains the N parallel interfering subcarriers.

Recall that $\mathbf{r}^{(A)}$ and $\mathbf{r}^{(B)}$ denote the original input vectors to N-point FFTs which are synchronized to TX A and TX B frequencies, respectively. Then, at the ith iteration of the proposed scheme, they are replaced by $\mathbf{r}^{(A,i)}$ and

$\mathbf{r}^{(B,i)}$, respectively, which are the updated versions given as follows:

$$\mathbf{r}^{(A,i)} = \mathbf{r}^{(A)} - \text{IFFT}\left[H_{1,1}^{(B)}\hat{X}_{1,1}^{(B,i)}, H_{1,2}^{(B)}\hat{X}_{1,3}^{(B,i)}, \cdots, H_{N_b,n_c}^{(B)}\hat{X}_{N_b,n_c}^{(B,i)}\right] \odot \left[e^{\frac{-j2\pi\varepsilon}{N}}, e^{\frac{-j2\pi 2\varepsilon}{N}} \cdots e^{-j2\pi\varepsilon}\right] \tag{31}$$

$$\mathbf{r}^{(B,i)} = \mathbf{r}^{(B)} - \text{IFFT}\left[H_{1,1}^{(A)}\hat{X}_{1,1}^{(A,i)}, H_{1,2}^{(A)}\hat{X}_{1,3}^{(A,i)}, \cdots, H_{N_b,n_c}^{(A)}\hat{X}_{N_b,n_c}^{(A,i)}\right] \odot \left[e^{\frac{j2\pi\varepsilon}{N}}, e^{\frac{j2\pi 2\varepsilon}{N}} \cdots e^{j2\pi\varepsilon}\right]. \tag{32}$$

In (31) and (32) , $\hat{X}_{\beta,m}^{(A,i)}$ and $\hat{X}_{\beta,m}^{(B,i)}$ denote the estimated versions of $X_{\beta,m}^{(A)}$ and $X_{\beta,m}^{(B)}$, respectively, at the ith iteration, $\left[e^{\frac{-j2\pi\varepsilon}{N}}, e^{\frac{-j2\pi 2\varepsilon}{N}} \cdots e^{-j2\pi\varepsilon}\right]$ and $\left[e^{\frac{-j2\pi\varepsilon}{N}}, e^{\frac{-j2\pi 2\varepsilon}{N}} \cdots e^{-j2\pi\varepsilon}\right]$ denote the sampled versions of the residual complex exponentials by CFO, and $\odot$ denotes the element-wise multiplication. Note that the term $\text{IFFT}\left[H_{1,1}^{(B)}\hat{X}_{1,1}^{(B,i)}, H_{1,2}^{(B)}\hat{X}_{1,3}^{(B,i)}, \cdots, H_{N_b,n_c}^{(B)}\hat{X}_{N_b,n_c}^{(B,i)}\right] \odot \left[e^{\frac{-j2\pi\varepsilon}{N}}, e^{\frac{-j2\pi 2\varepsilon}{N}} \cdots e^{-j2\pi\varepsilon}\right]$ in (31) corresponds to the reconstructed time domain-sampled signal from TX antenna B to the received signal synchronized to TX antenna A. The similar remark holds for (32).

In order to prove that the time domain ICI cancelation of the proposed scheme is identical to the frequency (subcarrier) domain cancelation, let us expand (31) first. We denote the nth output of IFFT, i.e., $\text{IFFT}\left[H_{1,1}^{(\text{B})}\hat{X}_{1,1}^{(\text{B},i)}, H_{1,2}^{(\text{B})}\hat{X}_{1,2}^{(\text{B},i)}, \cdots, H_{N_b,n_c}^{(\text{B})}\hat{X}_{N_b,n_c}^{(\text{B},i)}\right]$, by $\eta^{(\text{A},i)}(n)$, then $\eta^{(\text{A},i)}(n)$ for $1 \le n \le N$ is calculated as follows:

$$\eta^{(\text{A},i)}(n) = \frac{1}{N}\sum_{\beta=1}^{N_b}\sum_{m=1}^{n_c} H_{\beta,m}^{(\text{B})}\hat{X}_{\beta,m}^{(\text{B},i)} e^{-j2\pi((\beta-1)n_c+m)n/N} \tag{33}$$

For simplicity, we set $l = (\beta-1)n_c + m$, and then, (33) is expressed as

$$\eta^{(\text{A},i)}(n) = \frac{1}{N}\sum_{l=1}^{N} H_l^{(\text{B})}\hat{X}_l^{(\text{B},i)} e^{j2\pi nl/N}. \tag{34}$$

Then, to reconstruct the received signal from the other TX antenna (antenna B here) in the time domain, the sampled versions of the residual complex exponential term are multiplied to $\eta^{(\text{A},i)}(n)$. The nth sample of the received signal from the other TX antenna in the time domain is denoted by $\mathrm{i}^{(\text{A},i)}(n)$, and then, $\mathrm{i}^{(\text{A},i)}(n)$ is expressed as follows:

$$\begin{aligned}\mathrm{i}^{(\text{A},i)}(n) &= \eta^{(\text{A},i)}(n) \odot e^{-j2\pi n\varepsilon/N} \\ &= \frac{1}{N}\sum_{l=1}^{N} H_l^{(\text{B})}\hat{X}_l^{(\text{B},i)} e^{j2\pi n(l-\varepsilon)/N}.\end{aligned} \tag{35}$$

Denote the kth output of $\text{FFT}\left[\mathrm{i}^{(\text{A},i)}(1), \mathrm{i}^{(\text{A},i)}(2), \ldots, \mathrm{i}^{(\text{A},i)}(N)\right]$ by $F_k^{(A)}$, then $F_k^{(A)}$ for $1 \le k \le N$ is expressed as

$$\begin{aligned}F_k^{(A)} &= \sum_{n=1}^{N}\frac{1}{N}\sum_{l=1}^{N} H_l^{(\text{B})}\hat{X}_l^{(\text{B},i)} e^{j2\pi n(l-\varepsilon)/N} e^{-j2\pi nk/N} \\ &= \frac{1}{N}\sum_{l=1}^{N} H_l^{(\text{B})}\hat{X}_l^{(\text{B},i)}\sum_{n=1}^{N} e^{j2\pi n(l-k-\varepsilon)/N}.\end{aligned} \tag{36}$$

By using the summation formula for the geometric series, (36) is rewritten as

$$\begin{aligned}F_k^{(A)} &= \frac{1}{N}\sum_{l=1}^{N} H_l^{(\text{B})}\hat{X}_l^{(\text{B},i)}\frac{e^{j\pi n(l-k-\varepsilon)}\left(e^{-j\pi n(l-k-\varepsilon)} - e^{j\pi n(l-k-\varepsilon)}\right)}{e^{j\pi n(l-k-\varepsilon)/N}\left(e^{-j\pi n(l-k-\varepsilon)/N} - e^{j\pi n(l-k-\varepsilon)/N}\right)} \\ &= \sum_{l=1}^{N}\frac{\sin(\pi(l-k-\varepsilon))}{N\sin(\pi(l-k-\varepsilon)/N)} H_l^{(\text{B})}\hat{X}_l^{(\text{B},i)} \\ &= \sum_{l=1}^{N} Q(l-k-\varepsilon) H_l^{(\text{B})}\hat{X}_l^{(\text{B},i)}.\end{aligned} \tag{37}$$

By reusing the relation $l = (\beta-1)n_c + m$ and setting $k = (b-1)n_c + k'$, (37) is expressed as

$$F_k^{(A)} = \sum_{\beta=1}^{N_b}\sum_{m=1}^{n_c} Q\left((\beta-b)n_c + m - k' - \varepsilon\right) H_{\beta,m}^{(\text{B})}\hat{X}_{\beta,m}^{(\text{B},i)}. \tag{38}$$

From (38), we know that $F_k^{(A)}$ is finally equal to (7), and thus, it is proved that the proposed time domain cancelation is equivalent to the previous subcarrier domain cancelation.

Note that in each of (31) and (32), N, $N/2\log_2 N$, and N multiplications are required for IFFT input vector generation, N-point IFFT operation, and N-point complex sinusoid multiplication, respectively. In addition, we have to include the computations for two FFT blocks for the original OFDM demodulation which are now inside the cancelation loop (see Fig. 3a) unlike the previous subcarrier domain cancelation schemes (see Fig. 3b). Consequently, $4N + 2N\log_2 N$ multiplications are required in total at each iteration to reconstruct the interference in the time domain cancelation as shown in Table 1.

Table 1 The number of multiplications required in the operations for the interference term reconstruction at each branch per iteration of the proposed scheme

Operation	Number of multiplications
IFFT input vector generation	N
IFFT for time domain conversion	$\frac{N}{2}\log_2 N$
N-point complex sinusoid multiplication	N
FFT for the original OFDM demodulation	$\frac{N}{2}\log_2 N$
Total	$4N + 2N\log_2 N$

Note that as N increases to the practical range, the computational complexity of the proposed structure is proportional to $N \log_2 N$ whereas that of the previous scheme is proportional to N^2. Figure 9 and Table 2 compare the complexity between the previous subcarrier domain cancelation schemes and the proposed time domain cancelation scheme. It is remarkable that the proposed structure drastically reduces the complexity compared to the previous subcarrier domain cancelation schemes while maintaining the mathematical equivalence to the subcarrier domain cancelation schemes.

Table 2 Comparison of the number of multiplications between the previous and the proposed schemes according to N

N	Previous (frequency domain)	Proposed (time domain)	Proposed/previous
64	4096	1024	0.25
128	16,384	2304	0.14
256	65,536	5120	0.07
512	262,144	11,264	0.04
1024	1,048,576	24,576	0.02

5 Simulation results

In this section, we provide the simulation results to evaluate the performance of the proposed scheme. Commonly, we set $N = 256$. Regarding multi-path profile for generating $H_{b,k}^{(A)}$ and $H_{b,k}^{(B)}$, the number of multi-paths is 8 and their delays are distributed uniformly in $[0 \ T_{\max}]$ where $T_{\max}$ is the maximum delay spread. The guard interval is set to be larger than $T_{\max}$. The subcarrier spacing (=$1/T$ where T = OFDM symbol duration prior to the guard time insertion) is set to 15 kHz by referring to the Long-Term Evolution (LTE) standard. For the proposed AS (adaptive selective) scheme, the threshold value ρ is set to 0.4 regardless of the iteration number and the other parameters.

Figure 10 shows BERs of iterative ICI cancelation schemes according to the number of iterations i for $\varepsilon = 0.5$ with binary phase shift keying (BPSK) and $T_{\max} = T/100, T/50$, and $T/10$. The subblock size of FADAC-OFDM frame n_c is set to 8 irrespective of $T_{\max}$. We exclude the extremely frequency-selective fading channels where the optimal n_c of FADAC-OFDM is equal to 2, and then, the transmitter structure of FADAC-OFDM is trivially the same as that of CDAC-OFDM.

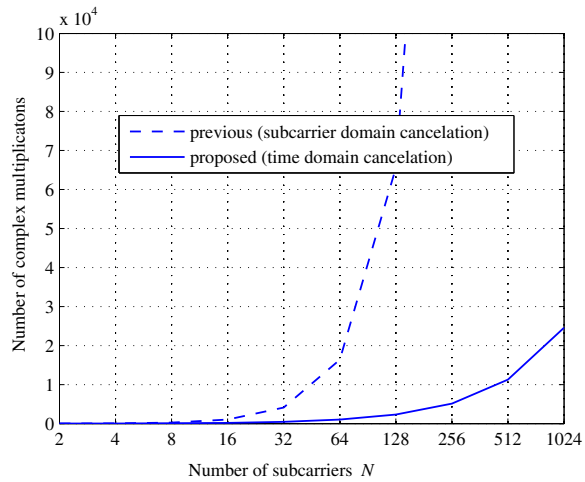

Fig. 9 Number of complex multiplications per iteration

As a baseline for the performance comparison, CDAC-OFDM with the iterative ICI cancelation using the entire detection symbols in the OFDM frame is included. Note that the iterative ICI cancelation results in almost no improvement to CDAC-OFDM. This is because the initial detection performance of CDAC-OFDM under frequency-asynchronous environment is poor, and thus, the ICI cancelation based on unreliable initial detection does not work properly. On the other hand, the iterative ICI cancelation works better for the case when it is applied to FADAC-OFDM which has a superb initial detection performance. However, the performance gain of ICI cancelation scheme in [10] is still not so significant. This scheme uses all the detected symbols in the interference reconstruction step without any consideration of the reliability of the detection symbols. Even in FADAC-OFDM, some of the detection symbols may eventually have relatively high possibility of errors due to severe ICI terms such as inter-block ICI as mentioned before. It is shown that after the first iteration, the performance fairly improves but from the second iteration, the performance is stuck in the same value. This is because the reconstructed interference term for cancelation is not updated anymore due to the erroneous portion of the constructed interference. Consequently, the performance gap between the scheme in [10] and the case of no ICI is still significant.

Note that two proposed schemes in this paper achieve significantly improved performance compared to the scheme in [10]. In the first iteration, the proposed DS scheme with $M = 1$ achieves a substantially decreased BER compared to the scheme in [10]. This implies that simply excluding the band edge subcarriers can efficiently avoid the erroneous ICI reconstruction. This results in the significant improvement by the canceling ICI from the rest of the subcarriers in the first iteration. However, the band edge subcarriers will not be canceled in the remaining iterations as well, and the BER converges to a still significantly higher level than that of the ICI-free case.

Meanwhile, the proposed AS scheme has significantly improved performance compared to the proposed DS scheme. Only within three or four iterations, the proposed AS scheme approaches nearly ICI-free level. This means

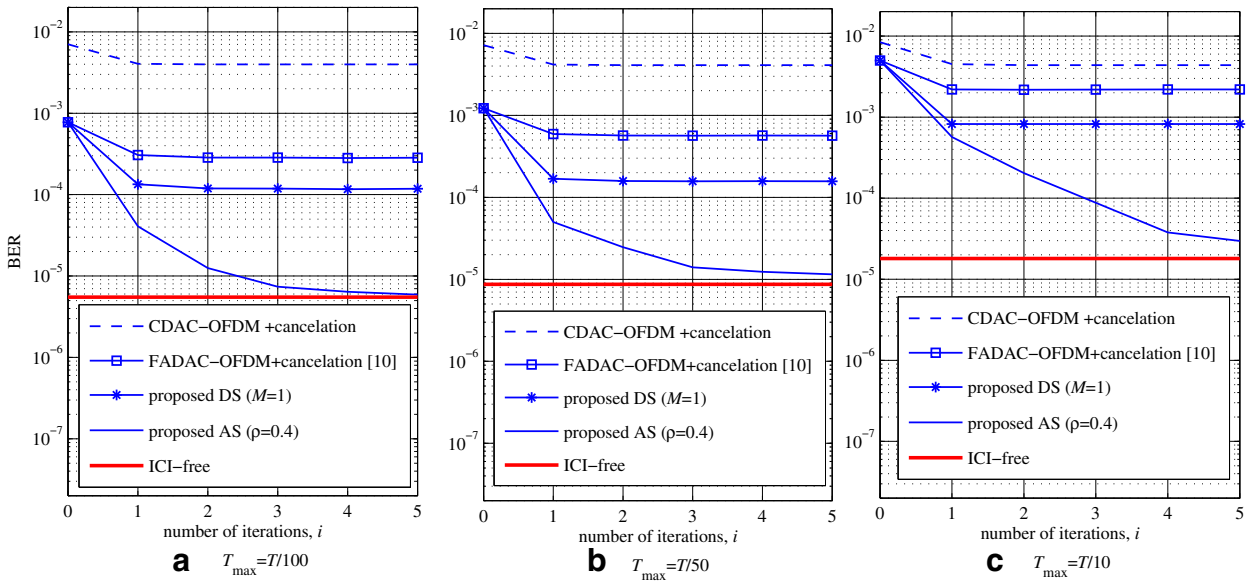

Fig. 10 a–c BER according to the number of iterations for $\varepsilon = 0.5$ and the several $T_{\max}$s with $n_c = 8$

that adaptively selecting the detection symbols for ICI reconstruction works properly, and as the iteration goes on, even the band edge subcarriers having high ICI power are gradually canceled. Despite the inferior performance of the proposed DS scheme to the proposed AS scheme, the proposed DS scheme has a merit that it is easy to implement and needs nearly no complexity overhead.

We can further improve the performances of the proposed schemes by more carefully optimizing or adaptively changing the system parameters such as the subblock size of FADAC-OFDM n_c, M for the proposed DS scheme, or ρ for the proposed AS scheme. However, we do not cover this case because the main point of this paper is to make sure of the improved performance of the proposed schemes even with suboptimal parameters. In addition, adaptively changing the system parameters is practically a burden in terms of system implementation.

Figure 11 shows BERs according to E_b/N_0 with $i = 4$ and $\varepsilon = 0.5$. From Fig. 10, i is set to 4 since the performances of all cases roughly converge at $i = 4$. The results for the schemes without ICI cancelation are also included to see the improvement by adding the iterative

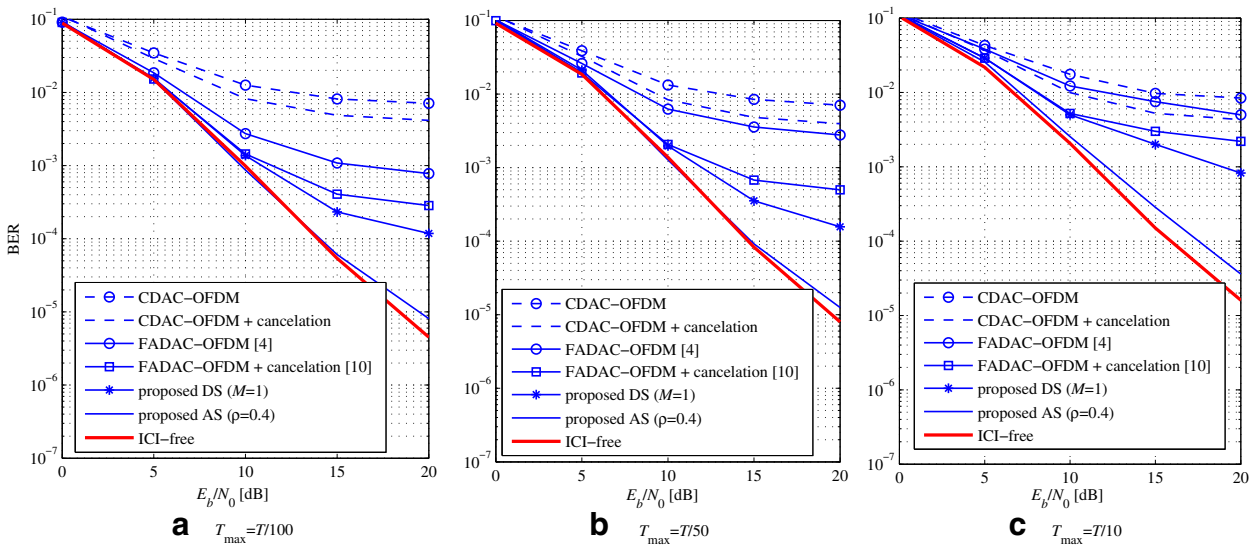

Fig. 11 a–c BER according to E_b/N_0 and $i = 4$ for several $T_{\max}$s and $\varepsilon = 0.5$ with $n_c = 8$

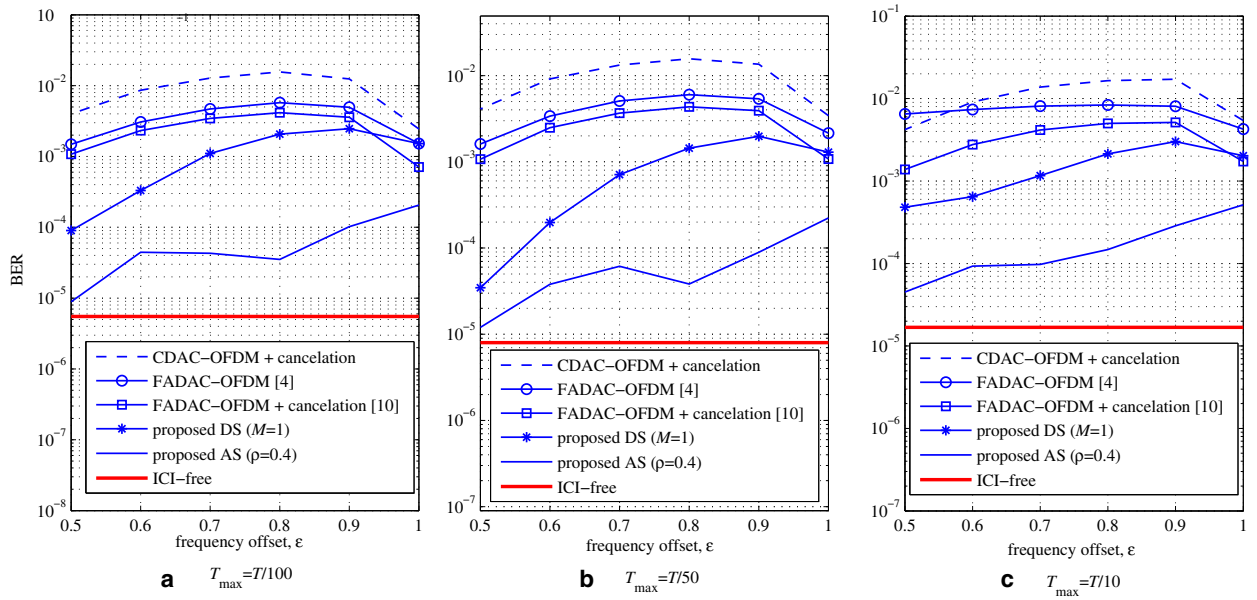

Fig. 12 a–c BER according to ε and $i = 4$ for several $T_{\max}$s with $n_c = 8$

ICI cancelation. Although there exist slight deviations in the high SNR region, the proposed AS scheme achieves nearly ICI-free performance with the fixed system parameters over the wide SNR range and the considered delay spread range.

In Fig. 12, the BER results are plotted for the large CFO (>0.5) cases. Although the performance gradually degrades and gets off from the ICI-free level as the CFO increases, the proposed schemes still attain the significant ICI reduction. Especially, the proposed AS scheme maintains the BER still in the meaningful level even for CFO >0.5. This is because the FADAC-OFDM basically holds its intrinsic feature, i.e., intra-block ICI self-cancelation irrespective of CFO although the inter-block ICI level increases as CFO increases. On the other hand, the ICI cancelation schemes to CDAC-OFDM abruptly break down as CFO gets larger than 0.5. For reference, see Fig. 5 in [6] and Fig. 5 in [7] which we cannot overlay on Fig. 12 in this paper as the system parameters and the channel parameters are not the same.

To investigate the performance under the practical situation, we also consider the case when there exists a channel estimation error. Figure 13 shows the BER results of each cancelation scheme according to the variance of the channel estimation error with $\varepsilon = 0.5, i = 4, E_b/N_0 = 20\,\text{dB}$, $T_{\max} = T/250$, and $n_c = 32$. The model of the imperfect channel estimation in [13] is employed, and the channel estimation error refers to the normalized one by the mean channel gain. The results show that performance degradation of the proposed scheme increases and the performance gaps among the schemes accordingly decrease as the variance of the error exceeds 0.2. Note however that in the practical range of the channel estimation error, say, lower than 0.2, all the schemes' performances are almost insensitive to the channel estimation error and thus the significant performance gap between the proposed AS scheme and the other schemes still remains the same.

6 Conclusions

We proposed an enhanced iterative ICI cancelation scheme distributed Alamouti-coded OFDM both in terms of the performance and the complexity. By avoiding the incorrect cancelation due to incorrect symbols, the proposed scheme achieves better performance than other ICI cancelation schemes. Only within three or four iterations,

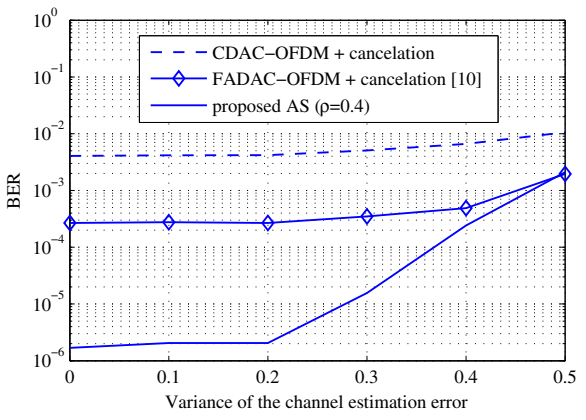

Fig. 13 BER according to the variance of the channel estimation error with $\varepsilon = 0.5, i = 4, E_b/N_0 = 20\,\text{dB}$, $T_{\max} = T/250$, and $n_c = 32$

the proposed scheme achieves near ICI-free performance by instantaneously reflecting the reliability of detection symbols at each iteration. As for complexity, by converting the ICI cancelation with functional equivalence, the proposed scheme has a drastically reduced computational complexity. The performance results shown in this paper sufficiently appeal as a promising solution for the current and future cooperative transmit antenna systems using OFDM waveform and Alamouti code. The proposed scheme will be further improved by combining with some sophisticated schemes, such as the adaptively selective cancelation based on the soft decision feedback [12]. We leave this as one of our future works.

Acknowledgements
This work was supported in part by the DGIST R&D Program of the Ministry of Science, ICT and Future Planning, Korea (17-IT-01), Basic Science Research Program through the National Research Foundation (2015R1D1A3A01015970) funded by the Ministry of Education, and the Information Technology Research Center support program (IITP-2016-R2718-16-0035) supervised by the Institute for Information & Communications Technology Promotion funded by the Ministry of Science, ICT and Future Planning, Korea.

Competing interests
The authors declare that they have no competing interests.

Author details
[1]Advanced Radar Technology Laboratory in DGIST, 333 Techno Jungang-daero, Hyeonpung-myeon, Dalseong-gun, Daegu, 42988, Republic of Korea. [2]Department of ICE in Yeungnam University, 280 Daehak-Ro, Gyeongsan, Gyeongbuk, 38541, Republic of Korea.

Received: 7 June 2016 Accepted: 1 February 2017
Published online: 23 February 2017

References

1. H Wang, XG Xia, Distributed space-frequency codes for cooperative communication systems with multiple carrier frequency offsets. IEEE Trans. Wirel. Commun. **8**(2), 1045–1055 (2009)
2. Z Li, XG Xia, An Alamouti coded OFDM transmission for cooperative systems robust to both timing errors and frequency offsets. IEEE Trans. Wirel. Commun. **7**(5), 1839–1844 (2008)
3. K Choi, Inter-carrier interference-free Alamouti-coded OFDM for cooperative systems with frequency offsets in non-selective fading environments. IET Commun. **5**(15), 2125–2129 (2011)
4. B Kim, K Choi, FADAC-OFDM: frequency asynchronous distributed Alamouti-coded OFDM. IEEE Trans. Vehi. Tech. **64**(2), 466–480 (2015)
5. Y Zhang, J Zhang, in *Proc. IEEE WCNC 2009*. Multiple CFOs compensation and BER analysis for cooperative communication systems, (2009), pp. 1–6
6. T Lu, H Lin, T Sang, in *Proc. IEEE ISPMRC 2010*. An SFBC-OFDM receiver to combat multiple carrier frequency offsets in cooperative communications, (2010)
7. J Lee, H Lin, T Sang, in *Proc. IEEE ISCAS 2012*. An SFBC-OFDM receiver with MLSE equalizer to combat multiple carrier frequency offsets, (2012)
8. Y Yao, X Dong, Multiple CFO mitigation in amplify-and-forward cooperative OFDM transmission. IEEE Trans. on Commun. **12**(60), 3844–3854 (2012)
9. K Lee, D Williams, in *Proc. IEEE GLOBECOM '00*. A space-frequency transmitter diversity technique for OFDM systems, (2000), pp. 1473–1477
10. B Kim, J Lee, D Jeong, K Choi, in *Proc. ITNG 2014*. Combining successive ICI cancelation to ICI suppressed Alamouti coded OFDM for frequency asynchronous distributed antenna systems, (2014)
11. OE Agazzi, N Seshardsi, On the use of tentative decisions to cancel intersymbol interference and nonlinear distortion (with application to magnetic recording channels). IEEE Trans. Inf. Theory. **2**(43), 394–408 (1997)
12. SH Muller, WH Gerstacker, JB Huber, in *Proc. GLOBECOM '96*. Reduced-state soft-output trellis-equalization incorporating soft feedback, (1996), pp. 95–100
13. Y Chen, C Tellambura, Performance analysis of maximum ratio transmission with imperfect channel estimation. IEEE Commun. Lett. **4**(9), 322–324 (2005)
14. B Zhou, Y Xiao, P Yang, S Li, in *Proc. WiCOM, 2011*. An iterative CFO compensation algorithm for distributed spatial modulation OFDM systems, (2011)
15. SM Alamouti, A simple transmitter diversity scheme for wireless communications. IEEE J. Select. Areas Commun. **16**(8), 1451–1458 (1998)
16. P Dharmawansa, N Rajatheva, H Minn, An exact error probability analysis of OFDM systems with frequency offset. IEEE Trans.Commun. **57**(1), 26–31 (2009)